REPORT DOCUMENTATION PAGE

Form Approved OMB NO. 0704-0188

1. REPORT DATE (DD-MM-YYYY)	2. REPORT TYPE	3. DATES COVERED (From - To)
	Old Reprint	-

4. TITLE AND SUBTITLE
Mechanical properties of the solid Li-ion conducting electrolyte: Li0.33La0.57TiO3

5a. CONTRACT NUMBER
W911NF-09-1-0451

5b. GRANT NUMBER

5c. PROGRAM ELEMENT NUMBER
611102

6. AUTHORS
Jeff Sakamoto, Yong-Hun Cho, Jeff Wolfenstine, Ezhiylmurugan Rangasamy, Hyunjoong Kim, Heeman Choe

5d. PROJECT NUMBER

5e. TASK NUMBER

5f. WORK UNIT NUMBER

7. PERFORMING ORGANIZATION NAMES AND ADDRESSES
Michigan State University
Hannah Administration Building
426 Auditorium Road, Room 301
East Lansing, MI 48824 -2612

8. PERFORMING ORGANIZATION REPORT NUMBER

9. SPONSORING/MONITORING AGENCY NAME(S) AND ADDRESS(ES)
U.S. Army Research Office
P.O. Box 12211
Research Triangle Park, NC 27709-2211

10. SPONSOR/MONITOR'S ACRONYM(S)
ARO

11. SPONSOR/MONITOR'S REPORT NUMBER(S)
57230-CH.21

12. DISTRIBUTION AVAILIBILITY STATEMENT
Approved for public release; distribution is unlimited.

13. SUPPLEMENTARY NOTES
The views, opinions and/or findings contained in this report are those of the author(s) and should not contrued as an official Department of the Army position, policy or decision, unless so designated by other documentation.

14. ABSTRACT
Li0.33La0.57TiO3 (LLTO) is a potential Li-ion conducting membrane for use in aqueous Li-air batteries. To be in this configuration its mechanical properties must be determined. Dense LLTO was prepared using a solidstate (SS) or sol–gel (SG) procedure and was hot-pressed to yield a high relative density material ([95 %). Young's modulus, hardness, and fracture toughness of the LLTO-SS and sol–gel LLTO-SG materials was determined and compared to other solid Li-ion conducting electrolytes. The Young's modulus for LLTO-SG and

15. SUBJECT TERMS
solid state, Li ion, battery, electrolyte,

16. SECURITY CLASSIFICATION OF:			17. LIMITATION OF ABSTRACT	15. NUMBER OF PAGES	19a. NAME OF RESPONSIBLE PERSON
a. REPORT	b. ABSTRACT	c. THIS PAGE			Lawrence Drzal
UU	UU	UU	UU		19b. TELEPHONE NUMBER 517-353-7759

Report Title

Mechanical properties of the solid Li-ion conducting electrolyte: Li0.33La0.57TiO3

ABSTRACT

Li0.33La0.57TiO3 (LLTO) is a potential Li-ion conducting membrane for use in aqueous Li-air batteries.
To be in this configuration its mechanical properties must be determined. Dense LLTO was prepared using a solidstate (SS) or sol–gel (SG) procedure and was hot-pressed to yield a high relative density material ([95 %). Young's modulus, hardness, and fracture toughness of the LLTO-SS and sol–gel LLTO-SG materials was determined and compared to other solid Li-ion conducting electrolytes. The Young's modulus for LLTO-SG and LLTO-SS was 186 ± 4 and 200 ± 3 GPa, respectively. The Vickers
hardness of LLTO-SG and LLTO-SS was 9.7 ± 0.7 and 9.2 ± 0.2 GPa, respectively. The fracture toughness, KIC, of both LLTO-SG and LLTO-SS was *1 MPa m1/2; the fracture toughness of LLTO-SG was slightly higher than that of LLTO-SS. Both LLTO-SG and LLTO-SS have a Young's modulus and hardness greater than the other possible solid Li-ion conducting membranes; Li7La3Zr2O12 and Li1?x?yAlxTi2-xSiyP3-yO12. Based on modulus and hardness hot-pressed LLTO exhibits sufficient mechanical integrity to be used as a solid Li-ion conducting membrane

REPORT DOCUMENTATION PAGE (SF298)
(Continuation Sheet)

Continuation for Block 13

ARO Report Number 57230.21-CH
Mechanical properties of the solid Li-ion conduc ...

Block 13: Supplementary Note

Approved for public release; distribution is unlimited.

J Mater Sci (2012) 47:5970–5977
DOI 10.1007/s10853-012-6500-5

Mechanical properties of the solid Li-ion conducting electrolyte: $Li_{0.33}La_{0.57}TiO_3$

Yong-Hun Cho · Jeff Wolfenstine · Ezhiylmurugan Rangasamy · Hyunjoong Kim · Heeman Choe · Jeff Sakamoto

Received: 18 February 2012 / Accepted: 12 April 2012 / Published online: 26 April 2012

Abstract $Li_{0.33}La_{0.57}TiO_3$ (LLTO) is a potential Li-ion conducting membrane for use in aqueous Li-air batteries. To be in this configuration its mechanical properties must be determined. Dense LLTO was prepared using a solid-state (SS) or sol–gel (SG) procedure and was hot-pressed to yield a high relative density material (>95 %). Young's modulus, hardness, and fracture toughness of the LLTO-SS and sol–gel LLTO-SG materials was determined and compared to other solid Li-ion conducting electrolytes. The Young's modulus for LLTO-SG and LLTO-SS was 186 ± 4 and 200 ± 3 GPa, respectively. The Vickers hardness of LLTO-SG and LLTO-SS was 9.7 ± 0.7 and 9.2 ± 0.2 GPa, respectively. The fracture toughness, K_{IC}, of both LLTO-SG and LLTO-SS was ~ 1 MPa $m^{1/2}$; the fracture toughness of LLTO-SG was slightly higher than that of LLTO-SS. Both LLTO-SG and LLTO-SS have a Young's modulus and hardness greater than the other possible solid Li-ion conducting membranes; $Li_7La_3Zr_2O_{12}$ and $Li_{1+x+y}Al_xTi_{2-x}Si_yP_{3-y}O_{12}$. Based on modulus and hardness hot-pressed LLTO exhibits sufficient mechanical integrity to be used as a solid Li-ion conducting membrane in aqueous Li-air batteries but, its fracture toughness needs to be improved without degrading its ionic conductivity.

Y.-H. Cho · H. Choe
School of Advanced Materials Engineering, Kookmin University, Jeongneung-gil 77, Seongbuk-gu, Seoul 136-702, Republic of Korea

J. Wolfenstine
Army Research Laboratory, RDRL-SED-C, 2800 Powder Mill Road, Adelphi, MD 20783, USA

E. Rangasamy · H. Kim · J. Sakamoto (✉)
Department of Chemical Engineering and Materials Science, Michigan State University, 2527 Michigan State University, East Lansing, MI 48824, USA
e-mail: jsakamot@msu.edu

Introduction

Lithium ion battery technology has advanced significantly in the last two decades. However, future energy storage demands will require safer, cheaper, and higher performance electrochemical energy storage [1, 2]. Examples of advanced energy storage technology based on Li include redox flow, molten alkali, and metal air batteries [1]. While there are numerous challenges in implementing these advanced technologies, they all require one component that has not yet been developed: a solid Li-ion conducting electrolyte. At present, a solid Li-ion conducting ceramic electrolyte has yet to be developed with the combination of high Li-ion conductivity, negligible electrical conductivity, chemical stability, and adequate mechanical integrity [3]. There are several ceramic Li-ion conducting electrolytes currently under investigation. For example, the NASICON family of electrolytes with the formula $Li_{1+x}Ti_{2-x}M_x(PO_4)_3$ (M = Al, Ga, In, Sc) [3] exhibits 0.3 mS/cm at room temperature. Another example includes the garnet family of electrolytes. Specifically, the garnet electrolyte with the nominal formulation of $Li_7La_3Zr_2O_{12}$ exhibits conductivity approaching 1 mS/cm at room temperature and stability in air and against Li. Perovskite ($Li_{0.33}La_{0.57}TiO_3$) is another example of a promising oxide electrolyte that also exhibits 1 mS/cm ionic conductivity and is stable in air and moisture [4–6]. It is important to note, however, that the high conductivity is only observed in the single crystal form, but not the polycrystalline form [7]. In the polycrystalline form, the more practical form, the conductivity significantly decreases due to high grain boundary resistance resulting in a total

conductivity in the 10^{-5} S/cm range [8]. Likewise, to limit cell polarization during cycling (0.1–1.0 mA/cm^2) a polycrystalline $Li_{0.33}La_{0.57}TiO_3$ electrolyte membrane must be in the 10–100 μm thick range [9]. Thus, a comprehensive assessment of the mechanical properties is required to determine if it is feasible to manufacture thin $Li_{0.33}La_{0.57}TiO_3$ membranes. Additionally, in the case of a liquid electrolyte in contact with a solid-state conductor, there is critical current density above which the solid electrolyte will fail or rapidly degrade in efficiency [10]. The critical current is a function of the fracture toughness to the 4th power [10, 11]. Therefore, it is very important to understand the mechanical properties of $Li_{0.33}La_{0.57}TiO_3$ to predict its behavior if it is to be used in aqueous Li-air batteries or other battery applications requiring a long operating life.

This paper reports on (1) the mechanical properties (elastic modulus, hardness, and fracture toughness) of dense $Li_{0.33}La_{0.57}TiO_3$ prepared by a solid-state or sol–gel procedure and hot-pressed to a high relative density (>95 %), and (2) a comparison between the mechanical properties of $Li_{0.33}La_{0.57}TiO_3$ with other possible solid-state Li-ion conducting membranes.

Experimental

Powder processing

$Li_{0.33}La_{0.57}TiO_3$ (LLTO) was chosen because this composition has one of the highest reported bulk Li-ion conductivities of the lithium lanthanum titanates [12, 13]. LLTO powders were synthesized using either a solid-state (LLTO-SS) or a sol–gel (LLTO-SG) procedure. Lithium carbonate (Puratronic 99.998 % Alfa Aesar), lanthanum(III) hydroxide (99.95 % Alfa Aesar) and titanium oxide (99.9 % Inframat Advanced Materials LLC) precursors were used as starting materials in the solid-state method. Stoichiometric amounts were added to an agate milling vial for mixing. A Retsch PM-100 planetary mill with agate milling media was used to mix the precursors. After mixing, the powders were collected and cold-pressed into pellets. The pellets were fired under air at 1000 °C for 4 h.

In the case of the sol–gel method, an LLTO sol–gel was synthesized from titanium(IV) isopropoxide (99.995 % from Alfa Aesar), lithium acetate (Reagent Grade from Sigma Aldrich), and lanthanum nitrate (99.9 % from Alfa Aesar) that was dissolved in chloroform and methanol (from Alfa Aesar). Titanium isopropoxide was dissolved in a chloroform solution and stirred for 30 min. Simultaneously, lithium acetate and lanthanum nitrate were dissolved in a methanol solution and stirred for 30 min. The lithium and lanthanum precursor solution was added slowly to the titanium solution. A gelation time of approximately 30–40 min was observed for the system. The gel was then placed in a jar and left to stand for 24 h before being opened for ambient drying, which was complete in 24 h. The ambient dried gel was then pre-calcined in air at 450 °C to remove any organics before further processing. The powders were then cold-pressed into pellets and fired under air at 1000 °C for 4 h.

Consolidation

Both the solid-state and sol–gel powders were consolidated by hot-pressing. LLTO pellets, 22 mm in diameter and 2 mm in thickness, were prepared by loading LLTO powders into a graphite die and heating them at 1000 °C under a 40 MPa pressure for 1 h under flowing argon. The resulting pellet was removed from the hot-pressing die and heated in air at 1000 °C for 4 h to burn off any residual graphite from the hot-pressing die and convert any surface Ti^{3+} back to Ti^{4+}. After heat-treatment, the pellet appeared white. The pellet was then mounted in crystal bond wax and cut into multiple parallelepipeds with a diamond saw for characterization and mechanical testing.

Characterization

X-ray diffraction (XRD, Cu Kα radiation) was used to characterize the phase purity before and after hot-pressing. The relative density of the hot-pressed samples was determined using three different methods. In the first method, the bulk density was determined from the mass and physical dimensions. In the second method, the bulk density was determined using the Archimedes method with water as the immersion fluid. The relative density was determined by dividing the bulk density by the theoretical density of $Li_{0.33}La_{0.57}TiO_3$ ($\rho_{theo} = 5.04$ g/cm^3) [14]. In the third method, the relative density was determined from the volume percent of porosity measured using image analysis. The microstructure of the hot-pressed LLTO samples was examined by optical and scanning electron microscopy (SEM). The grain size was determined from the SEM fracture surface images. For each specimen, 50 grains were selected randomly to calculate the mean grain size. For elongated grains, the mean diameter was calculated by averaging the largest and shortest diameters.

Mechanical testing

Young's modulus

The LLTO samples for mechanical testing were prepared using normal metallographic sample preparation techniques.

The Young's modulus, E, was determined using a nanoindentation method. The Young's modulus was determined from the load–displacement curve during unloading using the Oliver–Pharr method [15, 16]. A nanoindenter (G200, Agilent Technologies, Inc., Santa Clara, CA) with a Berkovich diamond tip was used to indent homogeneous regions of the sample's surface. Nine different tests were performed on each sample. The same test parameters were used for the solid-state and sol–gel LLTO specimens: 0.05 s^{-1} strain rate, 2 nm harmonic displacement target, and 45 Hz frequency. The maximum load used was 650 mN. Fused silica was used as the standard reference material to calibrate the instrument.

Hardness

The Vickers microhardness (H_v) and macrohardness were measured using a microhardness tester (Hardness testing machine, Mitutoyo Corporation, Japan) and a standard Rockwell hardness testing machine (Mitutoyo, Japan), respectively. The Vickers hardness of the hot-pressed LLTO specimens was measured at a load of 0.5 N for an indentation time of 15 s. A 1.6 mm diameter steel ball with a 100 kg major load was applied for the Rockwell hardness test of scale B (HRB). At least five hardness measurements were performed for each sample.

Fracture toughness

The fracture toughness, K_{IC}, of the hot-pressed LLTO samples was determined using the indentation technique [17–26]. A typical pyramid-shaped Vickers indenter was employed with a load of 0.3 kg for 15 s to induce cracks that extended from the indent corners, from which the crack sizes were determined optically. A total of at least five indents per sample were made to determine the fracture toughness.

Results and discussion

Structure

Figure 1 shows the XRD patterns of LLTO-SS and LLTO-SG materials after hot-pressing. From Fig. 1, the diffraction patterns of the LLTO-SS and LLTO-SG materials are similar, both reveal predominately single-phase LLTO. All LLTO peaks are indexed to a perovskite structure with the tetragonal $P4/mmm$ space group [14]. Rietveld analysis showed that the amount of second phase(s) in both materials was $<\sim 3$ wt %. The XRD patterns of the calcined and hot-pressed materials were similar, suggesting that there was no change in structure during the consolidation step.

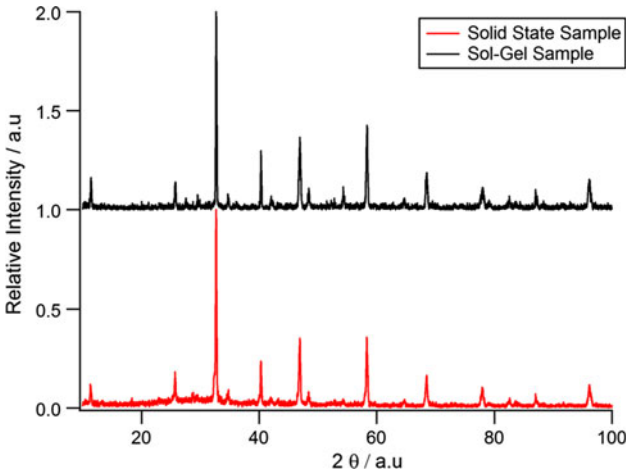

Fig. 1 XRD patterns of LLTO-SS and LLTO-SG after hot-pressing

Density

Three different density measurements were used and compared to determine the relative density of LLTO-SS and LLTO-SG materials due to the impact of density on the mechanical properties, such as hardness, Young's modulus, and fracture toughness, as shown in Table 1. The relative densities of the hot-pressed LLTO-SS and LLTO-SG materials were respectively, 97 ± 4 and 95 ± 5 % (the large scatter is due to the small size of the sample) using the Archimedes method, 98 ± 0.2 and 95 ± 0.4 % by physical measurements, and 99.9 ± 0.001 and 97.8 ± 0.02 % by image analysis. For all three measurements, the relative density of the hot-pressed LLTO-SS and LLTO-SG materials was above 95 %, with a slightly higher value for the LLTO-SS material. The relative density of the hot-pressed materials can be compared with the relative density of $Li_{0.33}La_{0.57}TiO_3$ consolidated only by conventional sintering at a similar temperature (1000 °C). Extrapolating the sintering data from Ban and Choi [8] to 1000 °C for 2 h $Li_{0.33}La_{0.57}TiO_3$ is predicted to have a relative density of only $\sim$50 %. The extrapolated sintering data reported by Yang et al. [14] at 1000 °C for 8 h also yielded a predicted relative density of $\sim$50 %. The much higher relative ($\sim$1.9×) density of the hot-pressed samples compared to the predicted values for the conventionally sintered samples was expected because the addition of applied stress

Table 1 Comparison of the relative density of LLTO-SG and LLTO-SS using (1) Archimedes method, (2) physical measurement, and (3) image analysis

Material	Archimedes method	Physical measurement	Image analysis
LLTO-SG	95 ± 5 %	94.7 ± 0.4 %	97.8 ± 0.02 %
LLTO-SS	96.9 ± 4 %	98.1 ± 0.2 %	99.9 ± 0.001 %

during hot-pressing increases the driving force for densification compared with that for conventional sintering [27].

Microstructure

Image analysis revealed a significant difference in the morphology of the pores between the LLTO-SG and LLTO-SS materials. In the LLTO-SG material relatively long, large pores were observed, whereas small round pores distributed uniformly were observed in the LLTO-SS material. Figure 2 shows typical fracture surfaces for the LLTO-SS and LLTO-SG materials. From Fig. 2 two important points are noted. Firstly, the fracture mode for LLTO-SG was predominantly intergranular, whereas it was a mixture of intergranular and transgranular for LLTO-SS. Secondly, the grain size of LLTO-SG was slightly larger (1.0 ± 0.4 μm) than that of LLTO-SS (0.8 ± 0.3 μm).

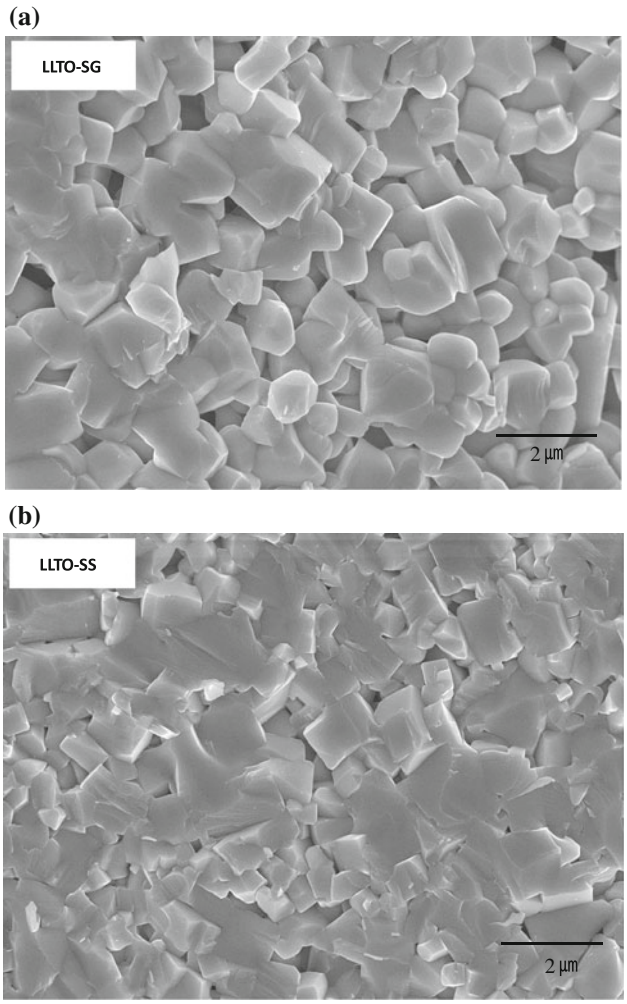

Fig. 2 SEM images of typical fracture surfaces of **a** LLTO-SG and **b** LLTO-SS

Young's modulus

The Young's modulus for the LLTO-SG and LLTO-SS materials determined by nanoindentation was 186 ± 4 and 200 ± 3 GPa, respectively: the Poisson's ratio for both materials was measured to be 0.25 using resonant ultrasound spectroscopy. For LLTO-SG, the Young's modulus was determined by resonant ultrasound spectroscopy to be ~192 GPa, confirming that the value determined by nanoindenation represents the true material value. The slight difference in modulus between LLTO-SG and LLTO-SS could be the result of microstructural variables, such as a mixture of phases, grain size, and porosity [28–34]. Young's modulus is expected to be independent of grain size at the grain size range used in this study [30, 34, 35]. Furthermore, as the grain size in both materials is similar (~1.0 vs. 0.8 μm), it is unlikely that the difference in modulus would be the result of a difference in grain size. One possible explanation might be the difference in the type and amount of second phases. It is unlikely that this caused the difference in modulus because the amount of second phases was low in both materials (<~3 wt%) and each had a common second phase ($La_2Ti_3O_9$). The elastic modulus is a function of the porosity; decreasing with increasing porosity [29–31, 34]. Therefore, it is possible that the slightly lower modulus of LLTO-SG compared to LLTO-SS was due to the higher porosity of LLTO-SG compared to LLTO-SS (Table 1).

The Young's modulus of LLTO-SG and LLTO-SS were compared with two other potential Li-ion conducting membrane materials (cubic $Li_7La_3Zr_2O_{12}$ [36–39] and $Li_{1+x+y}Al_xTi_{2-x}Si_yP_{3-y}O_{12}$ plate (where x and y are in the order of 0.1–0.3 [40–43]) for use in aqueous Li-air batteries. For cubic $Li_7La_3Zr_2O_{12}$ at a relative density of ~97 %, the Young's modulus determined by resonant ultrasound spectroscopy was 149.8 ± 0.4 GPa [40]. For an $Li_{1+x+y}Al_xTi_{2-x}Si_yP_{3-y}O_{12}$ plate (where x and y are on the order of 0.1–0.3) with a relative density of ~100 %, which was prepared using glass forming techniques, the Young's modulus determined by nanoindenation was 119 ± 2 GPa**.** Therefore, both LLTO-SG and LLTO-SS have a higher Young's modulus than $Li_7La_3Zr_2O_{12}$ and $Li_{1+x+y}Al_xTi_{2-x}Si_yP_{3-y}O_{12}$.

Hardness and bonding

The Vickers microhardness of LLTO-SG was 9.7 ± 0.7 GPa, whereas that of LLTO-SS was lower, 9.2 ± 0.2 HV, both of which are in good agreement with that of the previously reported hot-pressed $Li_{0.33}La_{0.57}TiO_3$ [41]. On the other hand, the macrohardness of the LLTO-SG material was 93 ± 5 HRB, whereas that of LLTO-SS was higher, 119 ± 2 HRB. Three major microstructural

features can control the hardness of these materials. The first is the difference in the type and amount of second phases but it is unlikely that this causes a difference in hardness because the amount of second phases is low in both materials ($<\sim 3$ at.%) and each has a common second phase ($La_2Ti_3O_9$). The second is the grain size. The hardness decreases with increasing grain size [33–35]. Therefore, it would be expected that LLTO-SS with a smaller grain size than LLTO-SG would exhibit higher hardness. The difference in grain size between the two materials, however, was not that large (~ 1.0 vs. 0.8 μm). The third variable is the porosity. Pores reduce the strength of a material by reducing the cross-section over which the load is applied and acting as stress concentrators [42]. Therefore, it is expected that LLTO-SS with a lower porosity (i.e., higher density) should have higher hardness. The macrohardness indeed showed the anticipated trend: LLTO-SG showed a lower Rockwell hardness than LLTO-SS (93 vs. 119 HRB). This is in agreement with the optical micrographs. The macrohardness of LLTO-SG material is influenced by large long pores (which are absent in LLTO-SS), whereas the microhardness is unaffected. The slightly higher microhardness of LLTO-SG suggests that it has a more consolidated microstructure, with a lower pore density in local regions than LLTO-SS. The reasons for this difference are not apparent, but might be the result of differences in the starting particle size and particle packing, and hence difference in interstitial void volume, or incomplete removal of organics in the sol–gel material [42, 43]. The hardness of LLTO-SG and LLTO-SS were compared with that of cubic $Li_7La_3Zr_2O_{12}$ and $Li_{1+x+y}Al_xTi_{2-x}Si_yP_{3-y}O_{12}$. The hardness of cubic $Li_7La_3Zr_2O_{12}$ and $Li_{1+x+y}Al_xTi_{2-x}Si_yP_{3-y}O_{12}$ was ~ 6.3 and ~ 7.8 GPa, respectively [40]. The hardness of both LLTO-SG and LLTO-SS was higher than that of cubic $Li_7La_3Zr_2O_{12}$ and $Li_{1+x+y}Al_xTi_{2-x}Si_yP_{3-y}O_{12}$.

Gilman [44] and Chin [45] reported that the ratio of the hardness, H, to the shear modulus, G, for cubic crystals is relatively constant for different types of bonding: For covalent, ionic and metallic bonding, $H/G \sim 0.1$, $H/G \sim 0.01$, and $H/G \sim 0.006$, respectively [44, 45]. The hardness and modulus data can be used to calculate the Gilman–Chen parameter (H/G) for LLTO, LLZO, and LATP to determine the dominant type of bonding within each. The shear modulus was estimated from the E values using the following equation, $G = E/2(1 + \nu)$, where ν is the Poisson's ratio [46]. This equation is based on the isotropic behavior, which is a good approximation because all three materials are polycrystalline [46]. A value of $\nu = 0.25$ was used to calculate G. The H/G value for LLTO-SG and LLTO-SS was ~ 0.13 and ~ 0.12, respectively, which suggests that dominant bonding type is covalent. This is in good agreement with results for other oxide perovskites [47], where the H/G value for LLZO is ~ 0.11, and for other oxide garnets [47], where the H/G value for LATP is ~ 0.16. This suggests that the major type of bonding in LATP is covalent. No data for this type of crystal class is available in the literature to compare with this value. The H/G values for LLTO, LLZO, and LATP were similar, suggesting that they all have the same type of dominant bonding: Covalent bonding.

Fracture toughness

Figure 3 shows typical Vickers indentations for the LLTO-SG and LLTO-SS materials. Both materials exhibit well-defined long straight cracks emanating from the corners of

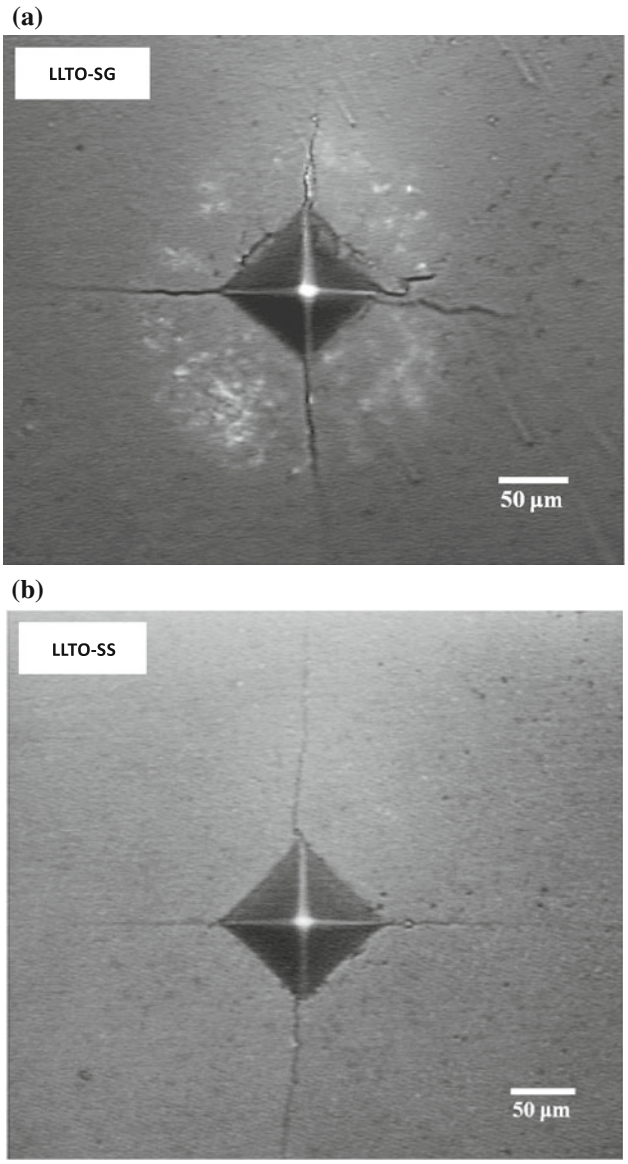

Fig. 3 Optical micrographs of a typical Vickers indentation on **a** LLTO-SG and **b** LLTO-SS

the indent. Table 2 lists the fracture toughness values of LLTO-SG and LLTO-SS using different equations to determine K_{IC} from the indentation crack lengths [17–26]. The long straight cracks are indicative of a brittle material [25–27]. For the both materials, the K_{IC} values were $\sim$1 MPa m$^{1/2}$. K_{IC} values for an ideal brittle material, glass, are close to unity [27, 43]. Therefore, the K_{IC} results suggest that LLTO-SG and LLTO-SS are brittle. Indeed, the K_{IC} values of $\sim$1 MPa m$^{1/2}$ for LLTO-SG and LLTO-SS are not surprising; ceramics are inherently brittle and extremely sensitive to flaws [25, 26]. In the absence of extrinsic shielding mechanisms (e.g., crack bridging), fracture in ceramic materials generally occurs catastrophically owing to their inherently low toughness of $\sim$1 to 3 MPa m$^{1/2}$ [25, 26]. Table 2 shows that the fracture toughness of LLTO-SG is slightly higher than that of LLTO-SS. To explain this difference, high high-magnification SEM images of the indentation crack profiles of LLTO-SG and LLTO-SS were investigated and are shown in Fig. 4. From Fig. 4 the crack path in LLTO-SG tended

Table 2 Analytical equations used for the K_{IC} calculation of LLTO-SG and LLTO-SS, where H is the Vickers hardness, d is half of the diagonal of the Vickers indent, C is the radius of the critical crack, E is the Young's modulus (with a Poisson's ratio value of 0.25), P is the load applied in the Vickers hardness test, and ϕ is a constraint factor ($\phi \sim 3$) [17]

References	K_{IC} Equation	K_{IC} (MPa m$^{1/2}$)	
		LLTO-SG	LLTO-SS
Evans and Charles [18]	$K_{IC} = 0.16Hd^2C^{-1.5}$	0.95 ± 0.11	0.89 ± 0.02
Laugier [19]	$K_{IC} = 0.01\left(\frac{E}{H}\right)^{\frac{2}{3}}\left(\frac{P}{C^{1.5}}\right)$	0.91 ± 0.06	0.67 ± 0.01
Anstis et al. [20]	$K_{IC} = 0.016\left(\frac{E}{H}\right)^{0.5}\left(\frac{P}{C^{1.5}}\right)$	0.890 ± 0.05	0.64 ± 0.01
Miyoshi et al. [21]	$K_{IC} = 0.018\left(\frac{E}{H}\right)^{0.5}\left(\frac{P}{C^{1.5}}\right)$	1.01 ± 0.05	0.72 ± 0.01
Ramachandran et al. [22]	$K_{IC} = 0.023\left(\frac{E}{H}\right)^{0.5}\left(\frac{P}{C^{1.5}}\right)$	1.29 ± 0.07	0.93 ± 0.01
Niihara et al. [23]	$K_{IC} = \frac{0.129}{\phi}\left(\frac{C}{d}\right)^{-1.5}Hd^{0.5}\left(\frac{E\phi}{H}\right)^{0.4}$	1.29 ± 0.09	1.27 ± 0.02
Lankford [24]	$K_{IC} = \frac{0.142}{\phi}Hd^{0.5}\left(\frac{C}{d}\right)^{-1.56}\left(\frac{E\phi}{H}\right)^{0.4}$	1.33 ± 0.09	1.31 ± 0.02

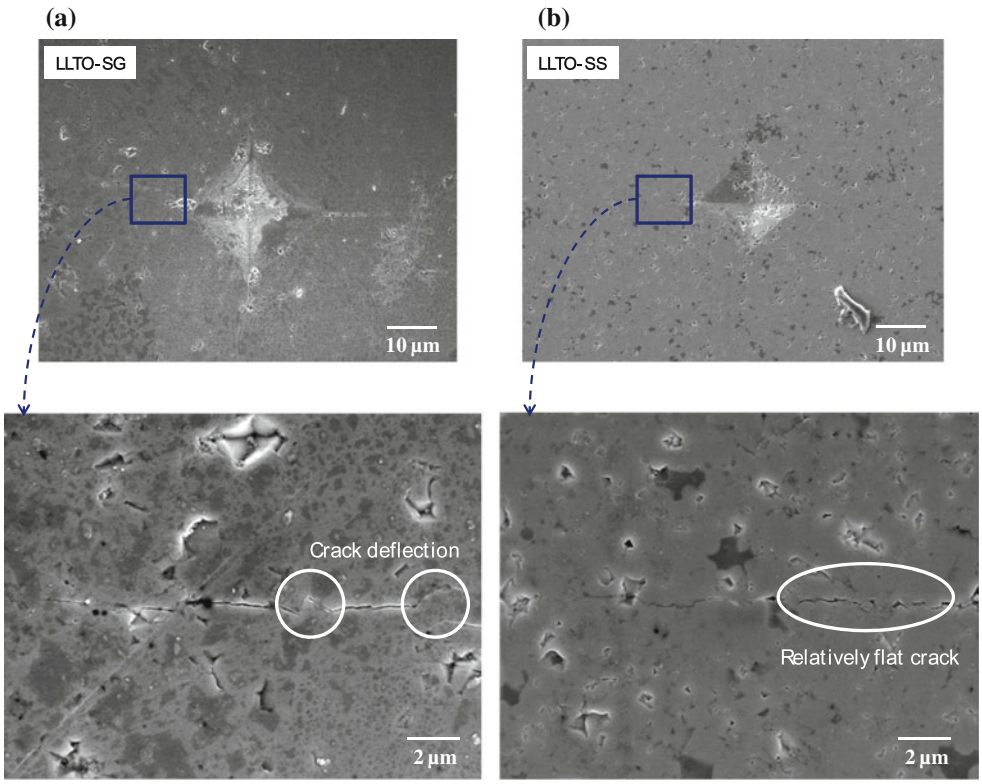

Fig. 4 SEM images of the Vickers indentation marks on **a** LLTO-SG and **b** LLTO-SS samples. Also shown is an enlarged view of one of the cracks emanating from a corner of an indent

to be more non-planar than that for LLTO-SS. The enhanced non-planar crack path in LLTO-SG is likely to have been caused by crack propagation along the weak grain boundaries. As a result, enhanced crack deflection occurs (as shown in Fig. 4), which leads to an increase in fracture toughness of LLTO-SG compared to LLTO-SS [27, 48–50]. This is in agreement with the observations in Fig. 2, where the fracture mode for LLTO-SG is almost completely intergranular compared to mixed intergranular and transgranular for LLTO-SS. There are several possible reasons for the difference in the crack propagation path and the fracture toughness of the two materials. A crack deflection mechanism is independent of the grain size but is a function of the grain morphology [48]. The grain morphology of LLTO-SG and LLTO-SS is similar. Therefore, the difference in fracture toughness of the two materials cannot be due to the grain morphology or the difference in grain size. Another possible microstructural variable could be the porosity. In general, the fracture toughness decreases with increasing porosity [51]. Therefore, one would expect LLTO-SS with lower porosity to exhibit higher fracture toughness but the opposite was observed. LLTO-SG with the higher porosity exhibited higher fracture toughness. The higher porosity in the LLTO-SG, particularly the long pores along the grain boundaries, alters the fracture path enough to the cause a part of the crack to propagate along the grain boundaries leading to crack deflection and higher fracture toughness [51]. Another possible reason for the difference in fracture toughness of the two materials could be the difference in processing (solid-state vs. sol–gel), which could lead to different grain boundary compositions and hence, different grain boundary fracture strengths. This cannot be verified without a detailed chemical analysis of the grain boundaries. Currently, there is no fracture toughness data available for cubic $Li_7La_3Zr_2O_{12}$ and $Li_{1+x+y}Al_xTi_{2-x}Si_yP_{3-y}O_{12}$ to compare to the LLTO-SS and LLTO-SG materials.

Conclusions

This study examined the mechanical properties (Young's modulus, hardness, and fracture toughness) of hot-pressed $Li_{0.33}La_{0.57}TiO_3$ prepared by a solid-state (LLTO-SS) or sol–gel (LLTO-SG) procedure. Hot-pressing at 1000 °C resulted in both LLTO-SS and LLTO-SG with relative densities >95 %. The Young's modulus for LLTO-SG and LLTO-SS determined by nanoindenation were 186 ± 4 and 200 ± 3 GPa, respectively. The Vickers hardness of LLTO-SG and LLTO-SS was 9.7 ± 0.7 and 9.2 ± 0.2 GPa, respectively. The fracture toughness, K_{IC}, of both LLTO-SG and LLTO-SS was ~ 1 MPa $m^{1/2}$; the fracture toughness of LLTO-SG was slightly higher than that of LLTO-SS. The higher fracture toughness of LLTO-SG was attributed to enhanced crack deflection along the grain boundaries compared to LLTO-SS. Both LLTO-SG and LLTO-SS have a Young's modulus and hardness greater than the other possible solid-state Li-ion conducting membranes; $Li_7La_3Zr_2O_{12}$ and $Li_{1+x+y}Al_xTi_{2-x}Si_yP_{3-y}O_{12}$. Based on stiffness and strength, hot-pressed LLTO exhibits sufficient mechanical integrity to be used as a solid Li-ion conducting membrane in aqueous Li-air batteries but the fracture toughness needs to be improved without degrading its ionic conductivity.

Acknowledgements This study was supported by the Priority Research Centers Program through the National Research Foundation of Korea (NRF) funded by the Ministry of Education, Science, and Technology (2009-0093814) and the National Research Foundation of Korea Grant (KRF-2008-313-D00012). JW would like to acknowledge the support of the U.S. Army Research Laboratory (ARL). Authors JS, ER and HK would like to acknowledge support from the Army Research Office (ARO).

References

1. Dunn B, Kamath H, Tarascon J-M (2011) Science 334:928
2. Bruce PG, Freunberger SA, Hardwick LJ, Tarascon J-M (2012) Nature Mater 11:19
3. Knauth P (2009) Solid State Ionics 180:911
4. Wolfenstine J, Allen JL (2008) J Mater Sci 43:7247. doi: 10.1007/s10853-008-3048-5
5. Thangadurai V, Weppner W (2006) Solid State Ionics 12:81
6. Inaguma Y, Chen LQ, Itoh M, Nakamura T, Uchida T, Ikuta H, Wakihara M (1993) Solid State Commun 86:689
7. Bohnke O (2008) Solid State Ionics 179:9
8. Ban CW, Choi GM (2001) Solid State Ionics 140:285
9. Brike P, Salam F, Döring S, Weppner W (1999) Solid State Ionics 118:149
10. Viswanathan L, Virkar A (1983) J Am Ceram Soc 66:159
11. Viswanathan L, Ikuma Y, Virkar A (1983) J Mater Sci 18:109. doi:10.1007/BF00543815
12. Inaguma Y, Chen LQ, Itoh M, Nakamura T, Uchida T, Ikuta H, Wakihara M (1993) Solid State Commun 86:689
13. Kawai H, Kuwano J (1994) J Electrochem Soc 141:L74
14. Yang KT, Wang JW, Fung KZ (2008) J Alloys Compd 458:415
15. Oliver WC, Pharr GM (1992) J Mater Res 7:1564
16. Oliver WC, Pharr GM (2004) J Mater Res 19:3
17. Yeheskel O, Albayrak IC, Anasori B, Barsoum MW (2011) J Eur Ceram Soc 31:1703
18. Evans AG, Charles EA (1976) J Am Ceram Soc 59:371
19. Laugier M (1985) J Mater Sci Lett 4:1539
20. Anstis GR, Chantikul P, Lawn BR, Marshall DB (1981) J Am Ceram Soc 64:533
21. Miyoshi T (1985) J Jpn Soc Mech 51:2489
22. Ramachandran N, Shetty DK (1991) J Am Ceram Soc 74:2634
23. Niihara K, Morena R, Hasselman DPH (1982) J Mater Sci Lett 1:13
24. Lankford J (1982) J Mater Sci Lett 1:493
25. Hutchinson JW (1989) In: Germain P, Piau M, Caillerie D (eds) Theoretical and applied mechanics. Elsevier, Amsterdam, pp 139–144
26. Launey ME, Ritchie RO (2009) Adv Mater 21:2103

27. Barsoum MV (1997) Fundamentals of ceramics. The McGraw-Hill Companies, Inc., New York
28. Kuriyama K, Saito S, Iwamura K (1979) J Phys Chem Solids 40:457
29. Kovacik J (1999) J Mater Sci Lett 18:1007
30. Kim HS, Bush MB (1999) Nanostruct Mater 11:361
31. Dole SL, Hunter O, Wooge CJ (1977) J Am Ceram Soc 60:488
32. Yamai I, Ota T (1993) J Am Ceram Soc 76:487
33. Spriggs RM (1962) J Am Ceram Soc 45:454
34. Chaim R, Hefetz M (2004) J Mater Sci 39:3057. doi:10.1023/B:JMSC.0000025832.93840.b0
35. Fryxell RE, Chandler BA (1964) J Am Ceram Soc 47:283
36. Shimonishi H, Toda A, Zhang T, Hirano A, Imanishi N, Yamamoto N, Takeda Y (2011) Solid State Ionics 183:48
37. Kumazaki S, Iriyama Y, Kim KH, Murugan R, Tanabe K, Yammato K, Hirayama T, Ogumi Z (2011) Electrochem Commun 13:509
38. Murugan R, Thangaduri V, Weppner W (2007) Angew Chem Int Ed 46:7778
39. Rangasamy E, Wolfenstine J, Sakamoto J (2012) Solid State Ionics 206:28
40. Ni JE, Case ED, Sakamoto J, Ranagasamy E, Wolfenstine (2012) J Mater Sci (submitted)
41. Kingery WD, Bowen HK, Uhlmann DR (1976) Introduction to ceramics, 2nd edn. Wiley, New York
42. Wolfenstine J, Allen JL, Read J, Sakamoto J, Gonalez-Doncel G (2010) J Power Sources 195:4124
43. Chiang YM, Birnie D, Kingery WD (1979) Physical ceramics. Wiley, New York
44. Gilman JJ (1960) Aust J Phys 13:327
45. Chin GY, Wernick JH, Geballe TG, Mahajan S, Nakahara S (1978) J Appl Phys 33:103
46. Barrett CR, Nix WD, Tetelman AS (1973) The principles of engineering materials. Prentice-Hall, Inc., Englewood Cliffs, NJ
47. Gilman JJ (2009) Chemistry and physics of mechanical hardness. Wiley, New York
48. Faber KT, Evans AG (1983) Acta Metall 4:565
49. Faber KT, Evans AG (1983) Acta Metall 4:577
50. Bower AF, Otitz M (1993) J Eng Mater Technol 115:229
51. Rice RW (1996) J Mater Sci 31:1969. doi:10.1007/BF00356616